Editors' Suggestion

Eulerian vs Lagrangian Irreversibility in an Experimental Turbulent Swirling Flow

Adam Cheminet,[1,*] Damien Geneste,[1] Antoine Barlet,[1] Yasar Ostovan,[2] Tarek Chaabo,[2] Valentina Valori,[1] Paul Debue,[1] Christophe Cuvier,[2] François Daviaud,[1] Jean-Marc Foucaut,[2] Jean-Philippe Laval,[2] Vincent Padilla,[1] Cécile Wiertel-Gasquet,[1] and Bérengère Dubrulle[1]

[1]*SPEC, CEA, CNRS, Université Paris-Saclay, CEA Saclay, F-91191 Gif-sur-Yvette, France*

[2]*Université Lille, CNRS, ONERA, Arts et Métiers ParisTech, Centrale Lille, FRE 2017-LMFL-Laboratoire de Mécanique des Fluides de Lille-Kampé de Fériet, F-59000 Lille, France*

(Received 2 November 2021; revised 13 April 2022; accepted 21 May 2022; published 14 September 2022)

In a turbulent fluid, the time-reversal symmetry is explicitly broken by viscosity, and spontaneously broken in the inviscid limit. Recently, Drivas [J. Nonlinear Sci. **29**, 65 (2019).] proved the equivalence of two different local indicators of time irreversibility: (i) an Eulerian one, based on regularity properties of the velocity field [Duchon and Robert, Nonlinearity **13**, 249 (2000).]; (ii) a Lagrangian one, based on symmetry properties of the trajectories under time reversal [Jucha *et al.*, Phys. Rev. Lett. **113**, 054501 (2014).]. We test this equivalence in a turbulent Von Kármán experiment at a resolution of the order of the Kolmogorov scale using a high resolution 4D-PTV technique. We use the equivalence to perform the first joined Eulerian-Lagrangian exploration of the dynamics leading to time irreversibility, and find that it is linked with vortex interaction, suggesting a link between irreversibility and singularity.

DOI: 10.1103/PhysRevLett.129.124501

In a viscous fluid, the energy dissipation is the signature of the breaking of the time-reversal symmetry $t \to -t$, $\mathbf{u} \to -\mathbf{u}$, where u is the velocity. This symmetry of the Navier-Stokes equations is explicitly broken by viscosity. Yet, in the limit of large Reynolds numbers, when the flow becomes turbulent, the nondimensional energy dissipation per unit mass becomes independent of the viscosity, meaning that the time-reversal symmetry is spontaneously broken. In classical equilibrium physics, spontaneous symmetry breaking is generally associated with singularities of the free energy. Viscous fluids are by nature out of equilibrium, so that no free energy can be *a priori* defined, and the physical origin of the spontaneous time-reversal symmetry breaking is still the subject of active research. In 1949, Onsager conjectured that this phenomenon could be triggered by the roughness of the velocity field, provided the flow is characterized by a Hölder exponent smaller or equal to $1/3$ [1–3]. In 2000, Duchon and Robert used an Eulerian energy balance to prove the conjecture for weak solutions of the Navier-Stokes equations [4]. This framework highlights a scalar quantity, $D(u)$, that only depends on the local velocity field and is the small scale limit of the energy flux through scale. $D(u)$ produces local nonviscous dissipation, in space and time, provided the velocity is singular enough. Being zero at the location of the regular velocity field, such a scalar therefore plays the role of an effective Eulerian "order parameter" for the time-reversal symmetry breaking. One may then add the viscous contribution to dissipation to get the total local energy dissipation.

Turbulence dynamics can also be considered following fluid particles trajectories. This is the so-called Lagrangian framework [5–7]. It is usually not straightforward to find the Lagrangian counterpart of Eulerian properties. In the case of time-reversal symmetry breaking, it has long been thought that the correct quantity was the instantaneous power $P = \mathbf{u} \cdot d\mathbf{u}/dt$ [8,9]. However, such single-point statistics is not sensitive to the energy flux through scale [8,10], which is believed to be a fundamental hallmark of irreversibility [11]. A relevant Lagrangian two point scalar quantity can be built using the symmetry property of the two-particle dispersion as a function of time [12]. Indeed, at short times, forward or backward time particle dispersion is different when time symmetry is broken [13,14]. Thus the difference between short time forward and backward two-particle dispersion corresponds to a Lagrangian effective order parameter of the time-reversal breaking [12,14–16].

An important step in the direction of understanding the building of irreversibility in turbulent flow was made recently by Drivas [17], who proved under suitable limits that the Eulerian and Lagrangian irreversibility indicators converge to the same quantity ϵ, the local energy dissipation. This result is interesting because it provides two different indicators, one Eulerian and one Lagrangian, that discriminate between regions where the fluid is or is not time irreversible. By tracking dynamically in time and space such regions, one may then get hints of the physical processes that are responsible for the symmetry breaking. In this Letter, we first test the equivalence of the two indicators on two different experimental setups of a von Kármán turbulent flow allowing us to probe the turbulence

roughly at the same measurement resolution but for two different Reynolds numbers. This requires time and space resolved simultaneous measurements of velocity fields and particles trajectories, which is an experimental challenge. We then use the equivalence to perform the first joined Eulerian-Lagrangian exploration of the dynamics leading to time irreversibility, and find that it is linked with vortex interaction, suggesting a link between irreversibility and singularity.

Experimental setups.—4D particle tracking velocimetry (PTV) measurements were performed at the center of two experiments: (i) a small von Kármán flow (SVK) with a radius $R = 0.1$ m and height 0.18 m [18,19]; (ii) a five time bigger Giant von Karman (GVK) flow, with radius $R = 0.5$ m and same aspect ratio [20]. Both tanks were filled with water (viscosity $\nu \approx 10^{-6}$) maintained at a constant $T = 20\ C$ temperature. The flow is forced by two counter-rotating impellers at frequency $F = 0.1$ Hz located at the upper and lower ends of the tank, resulting in a global Reynolds number $\mathrm{Re} = 2\pi R^2 F/\nu$. The average dissipation rate ϵ was computed from the torque measurements [21,22], to estimate the Kolmogorov length scale $\eta = (\nu^3/\epsilon)^{1/4}$ and timescale $\tau_\eta = (\nu/\epsilon)^{1/2}$. The different experimental parameters are summarized in Table I. Imaging of a cuboid ($40 \times 40 \times 6$ mm^3 for SVK and $50 \times 40 \times 6$ mm^3 for GVK) is performed using four high-speed cameras at the middle of both tanks. The volume is lighted by a 30 mJ pulse high speed Nd-YLG laser. Neutrally buoyant particles are added to the flow to act as tracers. Each sequence of measurement is made of 3226 consecutive time steps acquired with a acquisition frequency of 200 Hz for SVK and 1200 Hz for GVK. We perform statistics over 30 such sequences. 4D-PTV data were obtained through the DAVIS10 software using the "Shake-the-Box" algorithm [23]. They provide positions and trajectories in the volume per frame of about 49 000 particles in SVK and 70000 in GVK, resulting in a mean interparticle distance of $\Delta x_p \approx 1.8\eta$ for SVK and $\Delta x_p \approx 3.9\eta$ for GVK. Postprocessing was done using in-house codes. Additional details including references [24–29] are given in the Supplemental Material [30].

Lagrangian and Eulerian irreversibility indicators.—From the data, we compute the Eulerian and Lagrangian irreversibility indicators as follow. Starting from the Lagrangian measurements $\mathbf{X}_{t_0,t}(\mathbf{x})$, representing the position at time t of the particle that was at location $\mathbf{x}$ at time t_0, we compute the deviation $\delta_\mathbf{r}\mathbf{X}_{t_0,t}(\mathbf{x}) = \mathbf{X}_{t_0,t}(\mathbf{x}+\mathbf{r}) - \mathbf{X}_{t_0,t}(\mathbf{x})$. With this, we define the following scale dependent quantities:

$$\Delta_\ell^{\pm\tau}(\mathbf{x},t) = \int d\boldsymbol{\xi}\, \phi^\ell(\boldsymbol{\xi}) \|\delta_{\boldsymbol{\xi}}\mathbf{X}_{t,t\pm\tau}(\mathbf{x}) - \delta_{\boldsymbol{\xi}}\mathbf{X}_{t,t}(\mathbf{x})\|^2, \quad (1)$$

where $\phi(\boldsymbol{x})$, can be any standard mollifier or smoothing function compactly supported in the ball of radius ℓ such that $\int d\mathbf{r}\,\phi(\mathbf{r}) = 1$ and $\phi^\ell(\mathbf{r}) = \ell^{-3}\phi(\mathbf{r}/\ell)$. In this Letter, we used the local mean in the ball of radius ℓ as mollifier. The Lagrangian irreversibility indicator at scale τ and ℓ and at position x and time t is then given by $\mathcal{I}_\mathcal{L}^{\tau,\ell}(\boldsymbol{x},t) \equiv (\Delta_\ell^{-\tau} - \Delta_\ell^{\tau})/(4\tau^3)$. This indicator, first introduced by [17], is a local version of the indicator of [12].

From the Eulerian velocity measurement, $\mathbf{u}(\mathbf{x},t)$, we compute the velocity increment over a displacement $\mathbf{r}$ $\delta_{\boldsymbol{r}}\boldsymbol{u} = \mathbf{u}(\mathbf{x}+\mathbf{r},t) - \mathbf{u}(\mathbf{x},t)$. With this, we construct the following scale dependent quantities:

$$\mathcal{D}_I^\ell(\boldsymbol{x},t) = \frac{1}{4}\int d\boldsymbol{\xi}\, \nabla\varphi^\ell(\boldsymbol{\xi}) \cdot \delta_{\boldsymbol{\xi}}\boldsymbol{u}(\delta_{\boldsymbol{\xi}}\boldsymbol{u})^2, \quad (2)$$

$$\mathcal{D}_\nu^\ell(\boldsymbol{x},t) = \frac{\nu}{2}\int d\boldsymbol{\xi}\, \nabla^2\varphi^\ell(\boldsymbol{\xi})(\delta_{\boldsymbol{\xi}}\boldsymbol{u})^2, \quad (3)$$

with $\varphi^\ell(\boldsymbol{x}) = \ell^{-3}\varphi(\boldsymbol{x}/\ell)$, a Gaussian function. In the limit $\ell \to 0$, $\mathcal{D}_I^\ell(\boldsymbol{x},t)$ tends to $D(u)$, the nonviscous contribution to dissipation due to velocity roughness [4]. The Eulerian irreversibility indicator at scale ℓ and at position x and time t is then given by $\mathcal{I}_\mathcal{E}^\ell(\boldsymbol{x},t) \equiv \mathcal{D}_I^\ell + \mathcal{D}_\nu^\ell$.

The Drivas theorem [17] then states that for any sequence of weak solutions of the Navier-Stokes equation indexed by viscosity, that converges strongly as $\nu \to 0$, we have

$$\lim_{\ell\to 0}\lim_{\Delta x\to 0}\lim_{\tau\to 0}\lim_{\nu\to 0}\mathcal{I}_\mathcal{L}^{\tau,\ell}(\boldsymbol{x},t) = \epsilon(\boldsymbol{x},t), \quad (4)$$

with ϵ being given by

$$\epsilon(\boldsymbol{x},t) = \lim_{\ell\to 0}\lim_{\Delta x\to 0}\lim_{\nu\to 0}\mathcal{I}_\mathcal{E}^\ell(\boldsymbol{x},t). \quad (5)$$

Limits, measurement resolution, and probed scales.—The Drivas equivalence is based on mathematical limits, which obviously cannot be satisfied experimentally, because viscosities and resolutions are necessarily finite. Physically, sending first viscosity to zero means that we consider a

TABLE I. Table of parameters for the SVK and GVK. R is the radius of the tank, F the impeller rotating frequency, Re and Re_λ the global and Taylor Reynolds number, η and τ_η are the Kolmogorov length and time, $S_{t_{\tau_\eta}}$ the particle Stokes number, Δx_p the measurement resolution, $\ell^\mathcal{E}$ and $\ell^\mathcal{L}$, the probed scales for Eulerian and Lagrangian indicators.

	R (m)	F (Hz)	Re	Re_λ	η (mm)	τ_η (ms)	$S_{t_{\tau_\eta}}$	F_a (Hz)	$\Delta x_p/\eta$	$\ell^\mathcal{E}/\eta$	$\ell^\mathcal{L}/\eta$
SVK	0.1	0.1	6300	82	0.30	92	6.7×10^{-5}	200	1.8	3.6	10
GVK	0.5	0.1	157000	352	0.14	18	8.1×10^{-5}	1200	3.9	10	10

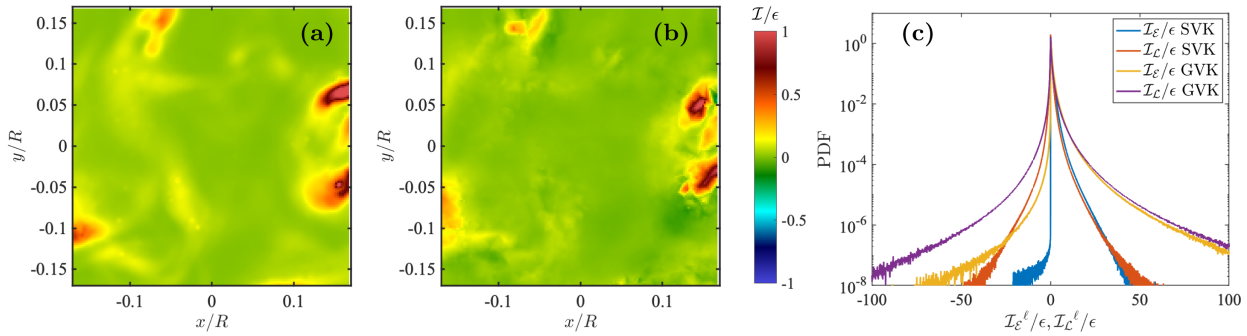

FIG. 1. Instantaneous snapshots of Eulerian (a) and interpolated-Lagrangian (b) irreversible criteria normalized by the mean energy dissipation ϵ, computed in the middle plane of the measurement volume of our SVK dataset. (c) PDFs of Lagrangian and Eulerian irreversible criteria for SVK and GVK.

situation where the velocity field is not regularized by viscosity [31], so that we are in the inertial range, which ends at a scale of the order 3 to 10 Kolmogorov scales. Therefore, we apply the following procedure: we first set the viscosity, then set the spatial resolution at a value $\Delta x/\eta \in [3, 10]$, and then choose the smallest value of $\ell > \Delta x$ ensuring either convergence of Lagrangian statistics, or sufficient denoising of the Eulerian quantities. It means replacing the triple limits $\lim_{\ell\to 0}\lim_{\Delta x\to 0}\lim_{\nu\to 0}$ in Eqs. (4) and (5) by $\lim_{(\ell/R)\to 0/\ell>\Delta x,\Delta x/\eta\in[3,10]}$. Given the Lagrangian and Eulerian resolution in each device, we used $\ell^\mathcal{E} = 3.6\eta$ for SVK and $\ell^\mathcal{E} = 10\eta$ for GVK while we obtained good statistical convergency for $\ell^\mathcal{L} = 10\eta$ in both SVK and GVK. Note that by going from the small experiment SVK to the large one, GVK, besides achieving a highest Reynolds number, we also achieve a ratio ℓ/R five time smaller, therefore improving the limit. Finally, to meet the $\tau \to 0$ limit, we use a fitting procedure: at each position and each time, we compute $(\Delta_\ell^{-\tau} - \Delta_\ell^\tau)$ for several $\tau = n\Delta_t$, with $n \in \{0, \ldots, 10\}$ and $\Delta_t = 1/F_a$. We then fit the function $(\Delta_\ell^{-\tau} - \Delta_\ell^\tau)$ by $A(x,t)\tau^3$, and get $\mathcal{I}_\mathcal{L}^{0,\ell}(x,t) = A(x,t)/4$. The fit was done on $11\Delta t$ to only keep trajectories of a least 21 time steps, thus limiting the noise due do erroneous smaller trajectories. In the sequel, we omit the time dependency of the Lagrangian criterion since we only focus at times $t \to 0$.

Instantaneous comparison and statistical analysis.—Figures 1(a) and 1(b) show an instantaneous comparison of both Eulerian and Lagrangian irreversibility criteria in the middle plane of our measurement volume taken from our SVK dataset. The Lagrangian criterion is interpolated linearly on the same mesh as the Eulerian criterion. There is a clear correlation between the two indicators, with the same spatial structures of intense irreversible and dissipative events, as well as the same range of values. The Lagrangian criterion is however more noisy, probably due to the sparse and inhomogeneous nature of the Lagrangian data. Furthermore, while two filters are applied for the Eulerian criterion, (B spline and the mollifier φ^ℓ), only one is used in the Lagrangian case (ϕ^ℓ).

A statistical comparison is provided in Fig. 1(c) showing Lagrangian and Eulerian PDFs for both SVK and GVK datasets. For positive values, the PDFs of both irreversibility criteria are quite similar. The Lagrangian criterion has stronger negative values than the Eulerian criterion for both flow cases. For SVK, the probed scale of the Eulerian indicator is quite close to the dissipative range, where the positive $\mathcal{D}_\nu^\ell$ term dominates explaining the low probability of negative Eulerian events—mostly due to noise. In comparison, this probability is higher for GVK where the probed scale is closer to the inertial range with stronger (upscale or downscale) interscale transfer. In both cases, the Lagrangian indicator has a higher probability of negative events. The Lagrangian criterion is, however, skewed towards positive values, a signature of turbulence irreversibility in average. Negative events corresponds to situations where forward dispersion is larger than backward dispersion. We have checked that such events correspond to meaningful trajectories, associated with trajectories around vortices or near stagnation points. Examples are provided in the Supplemental movies and in Fig. 3. Negative events nevertheless are forbidden by the Drivas theorem in the sense that the limit $\nu \to 0$, $\ell \to 0$, of the Eulerian dissipation—the limit of the Lagrangian indicator—should remain positive. This observation does not change when we go to a higher Reynolds number by increasing the size of our experiment, i.e., increasing the inertial range. We can then infer that negative events are caused by our finite value of viscosity, which sets an interesting constraints on the geometry of coherent structures in turbulence, see below. Finally, both indicators, though at roughly the same probed scale, increase in intensity with the Reynolds number. This is a signature of the multifractal character of the energy dissipation [31], resulting in a power-law increase of the variance with Re_λ, that was already observed for Lagrangian power [8]. Additional measurements are needed to quantify the corresponding exponent.

A finer test of the equivalence between irreversibility indicators is via the joint PDFs [Figs. 2(a) and 2(aa)]. Both joint PDFs are skewed towards the $x = y$ axis for positive

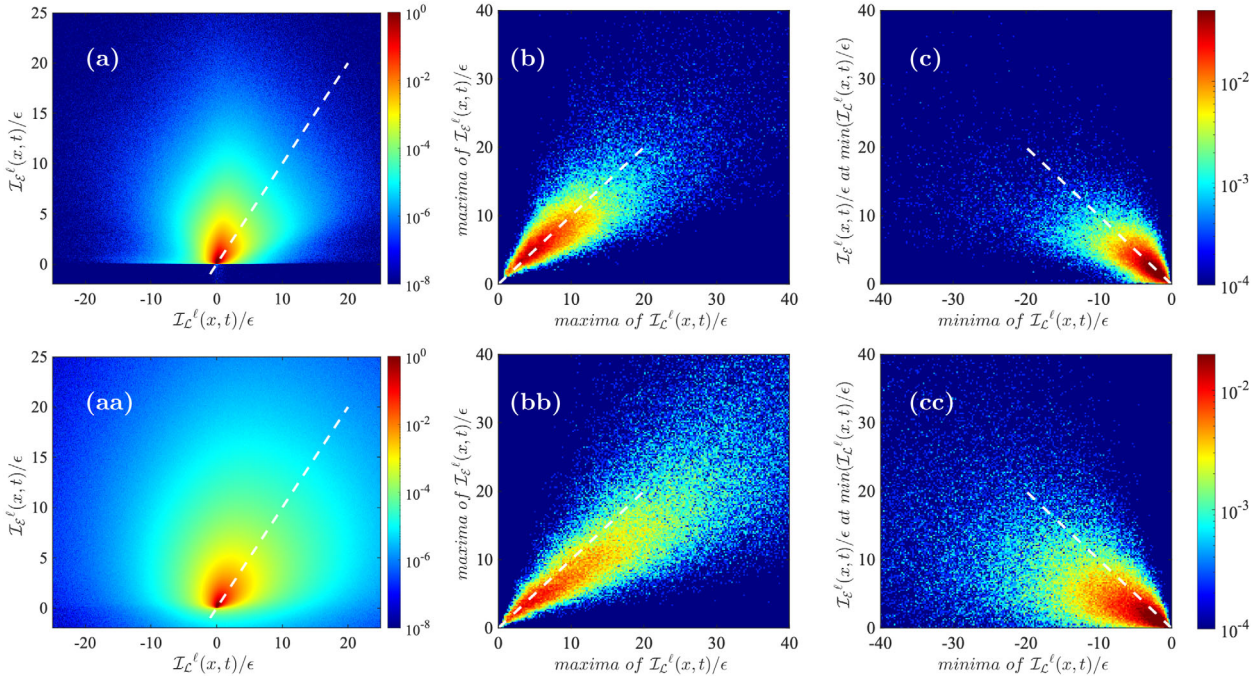

FIG. 2. Joint PDF of Lagrangian and Eulerian irreversibility indicators for SVK (a) and GVK (d). The dotted line has equation $y = x$. Joint PDF of Lagrangian and Eulerian maxima found at each snapshot for SVK (b) and GVK (e). Joint PDF of snapshot minima of the Lagrangian criterion and the corresponding value of the Eulerian criterion at the same position for SVK (c) and GVK (f).

values of Eulerian and Lagrangian irreversibility indicators, which shows that the two indicators tend to be equivalent for positive values. This trend is even more visible when comparing the indicators maxima of each 3D snapshots as shown in Figs. 2(b) and 2(bb). Furthermore, strong negative Lagrangian criteria are also relatively well correlated to positive Eulerian criteria of the same absolute intensity as seen in Figs. 2(c) and 2(cc). Such a correlation is not predicted by the Drivas theorem but confirms that highly irreversible Lagrangian trajectories occur at the locations of large Eulerian dissipation.

Discussion.—Our measurements show that, at a fixed resolution slightly above the Kolmogorov length scale, there is a clear correlation between Eulerian and Lagrangian irreversibility indicators when both are positive. This result does not change when increasing the Reynolds number from one order of magnitude. This result provides the first experimental confirmation of the Drivas theorem, and provides an interpretation of dissipation in terms of short time asymmetry between forward and backward pair dispersion. Whether such interpretation extends to asymmetry over a longer time scale and ballistic cascade phenomenology [32] is an open question. Our findings open a new perspective regarding the understanding of the building of the irreversibility. Indeed, we may combine both the Lagrangian and Eulerian criterion to understand where and how irreversible events form, and which particle trajectories are responsible for them. We then define a criterion to select a set I of strongly irreversible Lagrangian trajectories based on a thresholding procedure: a trajectory is in the set I if it includes a times t such that $|\mathcal{I}_\mathcal{L}^\ell(\boldsymbol{x}_n, t)| \geq T_*$. The selected trajectories are compared with isosurfaces of strong Eulerian irreversibility in Fig. 3. This particular event is the most intense event that we have over more than 96 000 snapshots corresponding to about $7000\tau_\eta$. The event corresponds to the interaction of two vortices at the edge of our measurement domain. The Eulerian irreversible areas can be seen at the

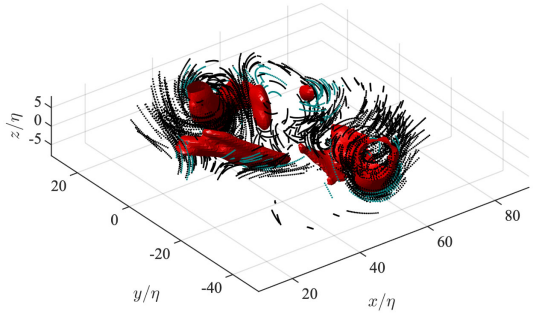

FIG. 3. 3D visualization of Eulerian irreversibility isosurfaces (in red) at $T_* \approx 6\epsilon$ and highly irreversible trajectories selected from the Lagrangian criterion with $T_* \approx 10\epsilon$. This event was taken from the SVK dataset. There are 19 time steps plotted for each trajectory. Positive Lagrangian indicators are showed in black as negative values are coded in blue-green. For representation purposes, the Lagrangian indicator was fitted on trajectory segments of $5\Delta t$. The Lagrangian scale is $\ell^\mathcal{L} = 10\eta$ and the Eulerian scale is $\ell^\mathcal{E} = 3.8\eta$.

edges of vortices or inside them, while the Lagrangian trajectories wind up around the vortices. We can also see a jet of flow from below interacting with the two vortices and separating in two directions, creating a stagnation point and a strong irreversible event, which is positive in the Eulerian framework, but negative in the Lagrangian framework as seen in Fig. 3. These events being bound to vanish in the inviscid limit, this sets interesting constrains about vortices interactions. We have observed similar features for at least the five strongest events in the SVK dataset. Temporal animations are provided in the Supplemental Material [30]. In any case, the correlation between highly irreversible Lagrangian and Eulerian areas, and vortex interaction suggests a possible link between irreversibility and singularity. Indeed, the close interaction of vortices frequently leads to vortex reconnection. High resolution numerical simulations [33] or ideal models of vortex reconnection based on Biot-Savart formula show the building of a singularity or quasisingularity at the location of vortex interaction [34,35]. The spontaneous breaking of irreversibility may then be interpreted as a nonequilibrium phase transition, mediated by a (quasi) singularity of the field itself. Whether this translates into a singularity of a suitable large deviation function (the nonequilibrium equivalent of a free energy) is an interesting open question.

This work was funded through ANR EXPLOIT, Grant Agreement No. ANR-16-CE06-0006 and ANR TILT Grant Agreement No. ANR-20-CE30-0035.

*adam.cheminet@cea.fr

[1] L. Onsager, Il Nuovo Cimento (1943–1954) **6**, 279 (1949).
[2] G. L. Eyink and K. R. Sreenivasan, Rev. Mod. Phys. **78**, 87 (2006).
[3] C. De Lellis and L. Szekelyhidi, J. Eur. Math. Soc. **16**, 1467 (2014).
[4] J. Duchon and R. Robert, Nonlinearity **13**, 249 (2000).
[5] A. Pumir, B. I. Shraiman, and M. Chertkov, Europhys. Lett. **56**, 379 (2001).
[6] N. Mordant, E. Lévêque, and J.-F. Pinton, New J. Phys. **6** 116 (2004).
[7] H. Xu, M. Bourgoin, N. T. Ouellette, and E. Bodenschatz, Phys. Rev. Lett. **96**, 024503 (2006).
[8] H. Xu, A. Pumir, G. Falkovich, E. Bodenschatz, M. Shats, H. Xia, N. Francois, and G. Boffetta, Proc. Natl. Acad. Sci. U.S.A. **111**, 7558 (2014).
[9] M. Cencini, L. Biferale, G. Boffetta, and M. De Pietro, Phys. Rev. Fluids **2**, 104604 (2017).
[10] G. Falkovich, H. Xu, A. Pumir, E. Bodenschatz, L. Biferale, G. Boffetta, A. S. Lanotte, and F. Toschi, Phys. Fluids **24**, 055102 (2012).
[11] R. Bitane, H. Homann, and J. Bec, Phys. Rev. E **86**, 045302(R) (2012).
[12] J. Jucha, H. Xu, A. Pumir, and E. Bodenschatz, Phys. Rev. Lett. **113**, 054501 (2014).
[13] G. Falkovich and A. Frishman, Phys. Rev. Lett. **110**, 214502 (2013).
[14] G. Falkovich, K. Gawędzki, and M. Vergassola, Rev. Mod. Phys. **73**, 913 (2001).
[15] S. Ott and J. Mann, J. Fluid Mech. **422**, 207 (2000).
[16] H. Xu, A. Pumir, and E. Bodenschatz, Sci. China Fluid Mech Astron. **59**, 1 (2016).
[17] T. D. Drivas, J. Nonlinear Sci. **29**, 65 (2019).
[18] P. Debue, V. Valori, C. Cuvier, F. Daviaud, J.-M. Foucaut, J.-P. Laval, C. Wiertel, V. Padilla, and B. Dubrulle, J. Fluid Mech. **914**, A9 (2021).
[19] Y. Ostovan, C. Cuvier, P. Debue, V. Valori, A. Cheminet, J.-M. Foucaut, J.-P. Laval, C. Wiertel-Gasquet, V. Padilla, B. Dubrulle *et al.*, in *Proceedings of 13th International Symposium on Particle Image Velocimetry* (Munich, Germany, 2019).
[20] P. Debue, Thesis, Université Paris-Saclay, 2019, https://tel.archives-ouvertes.fr/tel-02420454.
[21] D. Kuzzay, D. Faranda, and B. Dubrulle, Phys. Fluids **27**, 075105 (2015).
[22] F. Ravelet, L. Marié, A. Chiffaudel, and F. Daviaud, Phys. Rev. Lett. **93**, 164501 (2004).
[23] D. Schanz, S. Gesemann, and A. Schröder, Exp. Fluids **57**, 70 (2016).
[24] S. M. Soloff, R. J. Adrian, and Z.-C. Liu, Meas. Sci. Technol. **8**, 1441 (1997).
[25] B. Wieneke, Exp. Fluids **45**, 549 (2008).
[26] D. Schanz, S. Gesemann, A. Schreder, B. Wieneke, and M. Novara, Meas. Sci. Technol. **24**, 024009 (2013).
[27] P. H. C. Eilers and B. D. Marx, Stat. Sci. **11**, 89 (1996).
[28] S. Gesemann, F. Huhn, D. Schanz, and A. Schröder, in *18th Int Symp on Applications of Laser Techniques to Fluid Mechanics, Lisbon* (Lisbon, Portugal, 2016).
[29] A. Cheminet, Y. Ostovan, V. Valori, C. Cuvier, F. Daviaud, P. Debue, B. Dubrulle, J.-M. Foucaut, and J.-P. Laval, Exp. Therm. Fluid. Sci. **127**, 110376 (2021).
[30] See Supplemental Material at http://link.aps.org/supplemental/10.1103/PhysRevLett.129.124501 explains in details the experimental setup that we used, the post-processing that was done to obtain the Lagrangian and Eulerian velocity field as well as the physical meaning of the Eulerian irreversibility indicators.
[31] B. Dubrulle, J. Fluid Mech. **867**, P1 (2019).
[32] M. Bourgoin, J. Fluid Mech. **772**, 678 (2015).
[33] J. Yao and F. Hussain, J. Fluid Mech. **888**, R2 (2020).
[34] Y. Kimura and H. K. Moffatt, J. Fluid Mech. **834**, R1 (2018).
[35] H. K. Moffatt and Y. Kimura, J. Fluid Mech. **887**, E2 (2020).